DEVELOPMENT OF 61-CHANNEL DIGITAL BEAM-FORMING (DBF) TRANSMITTER ARRAY FOR MOBILE SATELLITE COMMUNICATION

G. Liang, W. B. Gong, H. J. Liu, and J. P. Yu

Shanghai Engineering Center for Microsatellites
Chinese Academy of Science
865 Changning Road, Shanghai 200050, China

Abstract—An 61-channel digital beamforming transmitter array antenna used in mobile satellite communication is presented in this paper. It can steer 16 beams simultaneously. The interface, architecture and subunits are described in detail. Standard hexagonal array (SHA) and 61-channel RF front ends are designed. Genetic Algorithm is adopted to realize the pattern synthesis with muti-objective optimization. The signal flow and hardware platform of the digital beamforming network are discussed, which can complete the high speed array signal processing with maximum throughput of 34.16 Gbps. A novel calibration scheme with high feasibility of project implementation is also proposed. The measurements of array antenna match well with simulation result, which validates the rationality and feasibility of the algorithms.

1. INTRODUCTION

Compared with conventional mechanically steering antennas, phased array antenna could provide significant improvement, which enjoys the benefits of flexible antenna pattern control and simultaneous multi-beam forming capabilities [1]. The phased array antenna with multi-beam pattern could enhance the performance of wireless communication systems in terms of capacity, coverage, and throughput by spatial filtering. Therefore, phased array antenna has become an essential part of future mobile satellite communication system [2, 3].

There are two ways to realize phase and amplitude control in phased array antenna. One is analog beamforming (ABF) method;

Corresponding author: G. Liang (hnlg219@163.com).

the other is digital beamforming(DBF) method. DBF array has many advantages over analogue beamforming method, with the most important benefits being:

- Beam steering in DBF systems can simply be achieved by using signal processing techniques in the digital domain, which reduces the need for the components utilized in ABF system such as phase shifters, time delay lines and attenuators.
- Precision in phase and amplitude control.
- Easy calibration of array and RF front ends in digital domain.
- Possibility of reconfiguration in orbit [4, 5].

This paper presents a digital beamforming transmitter array for mobile satellite communication, which was designed to steer sixteen independent beams with 61 independent channels simultaneously. As far as beam number is concerned, this array has the most number of beams in DBF array antenna for mobile satellite communication in China. The DBF array consists of array antenna, RF front ends, digital beamforming network and calibration unit. The interconnect architecture and interface are discussed. Genetic Algorithm with muti-objective optimization is adopted to realize the pattern synthesis of sixteen beams. The implementation of DBF array has several technological challenges. The first one is large throughput of digital beamforming network (BFN). The data transfer rate, between BFN and RF front-ends, is $61 \times 40\,\text{MSPS} \times 14 = 34.16\,\text{Gbps}$. A novel distributed structure with real signal processing for BFN is proposed in this paper, and the signal flow and hardware platform of BFN is described in detail. The second one is the gain and phase error of RF front-end channels, and a calibration scheme with high feasibility is discussed in detail. Ultimately, the DBF array was measured in an anechoic chamber, and the measurements show good agreement with the simulation results.

2. INTERFACE AND ARCHITECTURE OF DBF ARRAY

The block diagram of a DBF antenna for transmitting is shown in Fig. 1. First, the analog signals of sixteen beams at IF 70 MHz or 30 MHz are digitized to 12-bit digital signals by A/D converters with a 40 MHz sampling clock rate, and each beam has an instantaneous bandwidth of 10 MHz. Then, 16-channel digitized signals are transferred to digital beamforming network, which consists of orthogonal transform unit and digital beamforming computer. After orthogonal transform unit, we can get the I and Q extraction of sixteen beams. The complex signals of sixteen beams are fed

Figure 1. Block diagram of DBF transmitter antenna.

to digital beamforming computer, where the phase and amplitude adjustment of 16 beams are controlled precisely. The phase and amplitude excitation coefficients are calculated previously utilizing Genetic Algorithm according to the predefined antenna pattern. In the digital beaforming computer, 16 beams are synthesized simultaneously into 61 channels [6]. Then a calibration section is designed to calibrate 61 channels' Amplitude-frequency and Phase-frequency response in digital domain for the consistency of 61 channels. The calibrated signals of 61 channels are transformed to analogue signal by DACs at the speed of 40 M samples per second, and then up-converted to transmitting frequency (S band) by 61 RF front ends. RF front end is composed of up-converter, band-pass filter and power amplifier. The 61 RF front ends are mounted on the metal plane to dissipate the heat generated by the power amplifier of RF front end (approximately 5 W per channel). The metal plane is also used as the ground plane of array antenna, which carries the antenna patches on the topside. Through SMA Cable, RF front end can be plugged into antenna element, and the Plug-and-play design can cut down the insertion loss [7]. Ultimately, the signals are transmitted by radiating elements, some of which feedback to calibration unit to calculate the amplitude and phase error among 61 channels.

3. RADIATION PATTERN SYNTHESIS OF SHA

The DBF antenna array consists of 61 radiation elements which are arranged in a standard hexagonal array (SHA), and the distance between adjacent antenna elements is a half wavelength. Standard hexagonal array can reduce the amount of antenna elements by 13.4% when the radiated beams of antenna appear in conical area

perpendicular to the array, which has been proved by Sharp [8, 9].

Figure 2. Photograph of SHA and RF front ends.

SHA consists of 61 microstrip patch elements, which are printed on dielectric substrate, with electrical characteristics $\varepsilon_r = 8.8$, $\tan \delta = 0.0022$ and thickness $h = 2\,\text{mm}$. The microstrip patch radiator is covered by radome, made of FR4 material. The structure and material of antenna elements are fit for the application of LEO satellite in the space surroundings [10, 11]. The whole structure is mounted on a planar aluminum surface. Radiators are fed through coaxial probes, which run through aluminum surface and dielectric substrate, and connect with the female SMA cable of RF front end. The photograph of SHA is shown in Fig. 2.

The radiation pattern of each antenna element was simulated, and the typical case of 61 elements is presented in Fig. 3. The peak gain can reach $5\,\text{dB}$ and the radiated gain stays above $-3\,\text{dB}$ levels of its maximum value in the region $[-60°, 60°]$. Outside of this region, radiated gain is less than $-3\,\text{dB}$ level.

The far-field radiation pattern produced by standard hexagonal array can be expressed as

$$D(\theta) =$$

$$10\lg\left(\left|\sum_{i=1}^{61} A_i \exp\left(j^*\left(w_i + \frac{2\pi(\sin\theta(x_i\cos\varphi + y_i\sin\varphi))}{\lambda}\right)\right)\right|^2 \Big/ 61\right) + P(\theta) \quad (1)$$

where $P(\theta)$ is the radiation pattern of an individual element, A_i is excitation current amplitude, W_i is the excitation current phase, and λ is the transmitted wavelength. $[x_i, y_i]$ is the coordinates of the $[i, j]$ element and the Cartesian coordinates origin o is center element $[0, 0]$ [12–14].
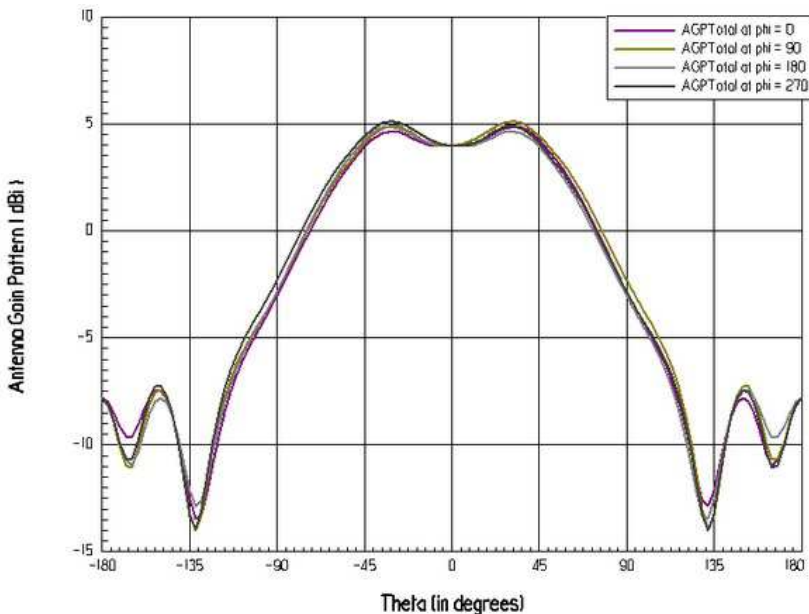
Figure 3. The simulated result of antenna element's radiation pattern.

However, phase-only excitation is adopted, because the amplitude excitation of sixteen beams may lead to the high PAPR (peak to average power ratio) level of the beamforming network's outputs, which are combined of amplitude-adjusted signals of 16 beams. As the transmitter antenna, the high PAPR level has great influence on the linear state of A-class power amplifier and results in the decrease of PA efficiency and the quality of communication further [12].

The main objective of antenna synthesis is to make the designed radiation pattern highly consistent with the ideal pattern. It could be achieved by adjusting the phase excitation coefficients. Genetic Algorithm (GA) is believed to have good performance on non-linear optimization [16]. But one of the key points in GA is the fitness function, we define the multi-objective fitness function as following

$$F(\theta, \varphi) = -[k_1 * |G(\theta, \varphi) - G_0| + k_2 * |SLL(\theta, \varphi) - SLL_0|] \qquad (2)$$

where $G(\theta, \varphi)$ and G_0 are the obtained and desired gain of main lobe respectively. $SLL(\theta, \varphi)$ and SLL_0 represent respectively the obtained and desired the side-lobe level of each beam, and k_1, k_2 are weighting coefficients to control the importance of the items described in the above equation. Appropriate weighting coefficients could make all the parameter of DBF array optimized [17–21].

(a)   (b)
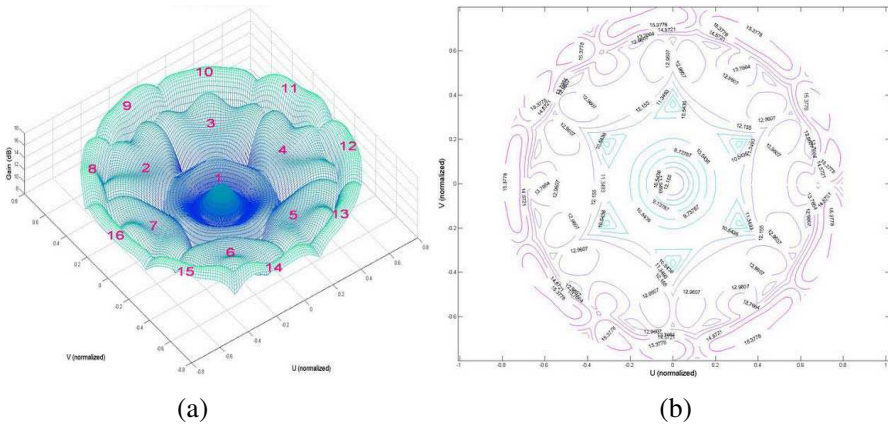
Figure 4. The simulation results: (a) 3D plots; (b) contour map.
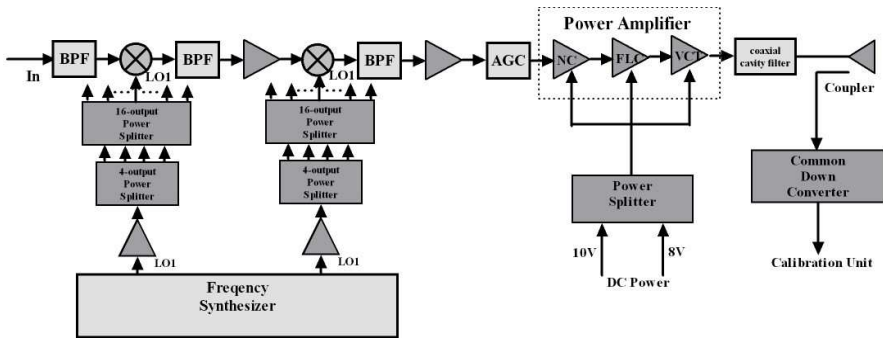
Figure 5. Block diagram of TX module.

Utilizing the $16 \times 61 = 976$ complex phase and amplitude excitation coefficients calculated by GA, the simulated radiation pattern of 16-beam DBF array is depicted in Fig. 4. Sixteen beams are arranged in three circles, six beams in the second circle, the rest in third circle, which is similar with the beam coverage of GlobalStar System.

4. RF FRONT ENDS

RF front ends consist of 61 TX modules. The TX module has a two-stage, double superheterodyne design. The block diagram of TX module is shown in Fig. 5.

The 61-channel IF signals, after the processing of calibration
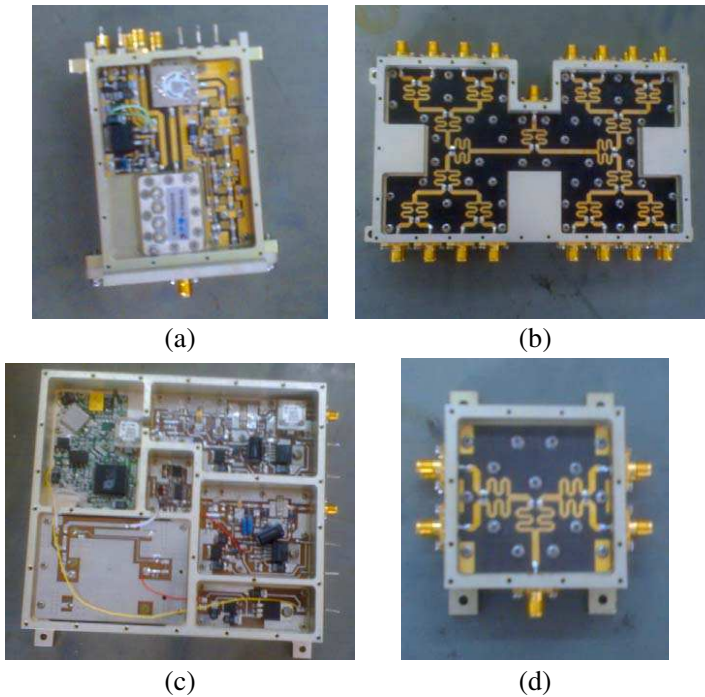
Figure 6. Photograph of subunits in RF front end: (a) TX module; (b)16-output power splitter network; (c) frequency synthesizer; (d) 4-output power splitter network.

unit, are transferred to TX modules at 10 MHz. First, the signals are filtered and up-converted to 170 MHz, and then passed through appropriate filter. The final up-conversion takes place at S band (2.2 GHz), after which the signals are filtered again and amplified by the PAs. The signal power of each individual channel is 5 W after PA. To get the carrier synchronization, all necessary LO signals are generated externally and fed to RF mixers by coaxial cable or on the PCBs of two dedicated power splitter network (one is 4-outputs power splitter network, the other is 16-outputs). Another dedicated power splitter is designed to supply the 61-channel TX modules with DC power. To get high quality of band rejection, a coaxial cavity filter is inserted between PA and antenna radiator. The subunits of TX module are shown in Fig. 6. The TX module exhibits a fairly constant magnitude response across the system bandwidth with a gain variation less than 1 dB, thus reduces the design difficulty of calibration unit.
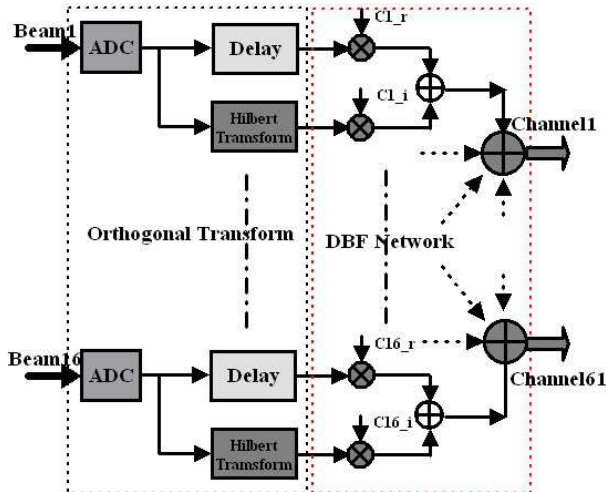
Figure 7. Block diagram of digital BFN.

5. DESIGN OF DIGTIAL BEAMFORMING NERWORK

5.1. Signal Processing of BFN

We have described the interface in Section 2, and the block diagram of digital beamforming network (BFN) is shown in Fig. 7.

First, the sixteen beams' signals, which have an instantaneous bandwidth of 10 MHz and centre at IF 70 MHz or 30 MHz, are band-pass sampled at a sample clock of 40 MHz. The sample rate not only satisfies the Nyquist criterion, but also aids further to ease the pressure of DSP. By sampling the input signal at 40 MHz, The centre frequency of sixteen beams can be aliased down to 10 MHz in digital domain.

The digital signals of sixteen beams are transferred to digital beamforming network (BFN). A generalized Digital BFN is presented, which performs the function of orthogonal transform and digital beamforming computer, as shown in Fig. 7.

The time-domain Hilbert Transform is designed to extract I and Q signals from the sampled signals. Since the frequency spectrum of input beam (FDM signal) is asymmetric, quadrature down-conversion is not preferred. If the sixteen beams are down-converted to baseband in quadrature down-conversion method, the aliasing frequency may occur and much more quadrature detection error will be produced compared with Hilbert Transform. Utilizing quadrature down-conversion, we need to design two branches of low-pass or band-pass filter to eliminate the image frequency of both I and Q extraction caused by down-

conversion, which could consume much more multiplier resources, compared with Hilbert Transform. As the input signals of sixteen beams are band-pass, Time-domain Hilbert Transform FIR filter (III type) is designed, which has the character of odd-symmetry property. The half-band structure for Time-domain Hilbert Transform FIR filter is proposed further, which can reduce the consumption of multiplier resource by 50%. Finally, the Hilbert Transform FIR filter with 31 orders is designed, which consumes merely 8 multipliers [16, 17]. The input beam is convolved with Hilbert Transform filter, and the result of convolution is Q extraction of input signals. To get I extraction, the input beam is digitally copied and delayed for several sample-time to compensate the time delay of Q extraction caused by Hilbert Transform, the delay time is calculated as

$$T = (N - 1)/2 * T_s \qquad (3)$$

where N is the order of Hilbert Transform filter, T_s is the sample-time of input digital signals.

After DFT filter bank, the complex signals of 16 beams are transferred to beamforming computer, expressed as vector

$$\overrightarrow{B_{1 \times 16}} = \left[\overrightarrow{B_1(n)}, \ \overrightarrow{B_2(n)}, \ \ldots \ldots \overrightarrow{B_{16(n)}} \right] \qquad (4)$$

The beamforming matrix of DBF network is

$$\overrightarrow{C_{16,61}} = \begin{vmatrix} C_{1,1} & C_{1,2} & \ldots \ldots & C_{1,61} \\ C_{2,1} & \ldots \ldots & \ldots \ldots & C_{2,61} \\ \ldots & \ldots & \ldots & \ldots \\ C_{16,1} & \ldots & \ldots & C_{16,61} \end{vmatrix}_{16*61}, \qquad (5)$$

where the cell $c_{i,j}$, which is calculated previously by GAdenotes the phase adjustment coefficient of the ith beam excitated by the jth channel. Within the digital beamforming computer, the sixteen beams are synthesized into sixty-one channels and then fed to 61 RF front-end channels, expressed as vector

$$\overrightarrow{T_{1 \times 61}} = \left[\overrightarrow{T_1(n)}, \ \overrightarrow{T_2(n)}, \ \ldots \ldots \overrightarrow{T_{61(n)}} \right] \qquad (6)$$

The 61-channel output results are calculated as following [18]

$$\overrightarrow{T_{1 \times 61}} = \overrightarrow{B_{1 \times 16}} \cdot \overrightarrow{C_{16,61}} =$$

$$\left[\sum_{i=1}^{16} \overrightarrow{B_i(n)} \cdot \overrightarrow{C_{i,1}}, \ \sum_{i=1}^{16} \overrightarrow{B_i(n)} \cdot \overrightarrow{C_{i,2}}, \ \ldots \sum_{i=1}^{16} \overrightarrow{B_i(n)} \cdot \overrightarrow{C_{i,16}} \right] \qquad (7)$$

The conventional complex signal processing is utilized in the existing digital BFN, which needs $16 \times 61 \times 4 = 3904$ multipliers to complete

the computation of beamforming computer. Thus, a novel real signal processing structure is proposed for the design of digital BFN, that is the real part of complex multiplier is merely adopted. The real part has contained all the messages of the input beam. After beamforming computation, the frequency spectrum of the real part corresponds well with that of the original input beam. RF front-ends don't use quadrature up-conversion structure, therefore we need not to transfer both I and Q extraction to 61 RF front-end channels. Because of the real signal processing, the consumption of multiplier hardware and the amount of transferred data can be reduced by 50%. However, the digital BFN still requires 1952 multipliers, distributed arithmetic (DA) algorithm is proposed further. Instead of using hardware multiplier, memory can be configured as look-up-table (LUT) to realize the multiplying computation, which is considered as software multiplier. DA algorithm is fit for Field Programmable Gate Array, which has abundant memory resources.

5.2. Hardware Platform of Digital Beamforming Network

Ultimately, a hardware platform of digital BFN is designed to validate the algorithm discussed above. Because of the high speed array signal processing, distributed process architecture is adopted and FPGA is selected to design the DBF network hardware architecture. The FPGA consists of DSP Block, Block RAM and LE resource, which can be configured as hardware multiplier and software multiplier to satisfy the multiplier-and-sum demand of beamforming network. And its distributed architecture and pins in plenty are fit for the parallel array signal processing [26, 27]. To reduce the effect of SEU, many anti-radiation technologies utilized on FPGA are adopted, such as TMR design and configuration data check by CRC code.
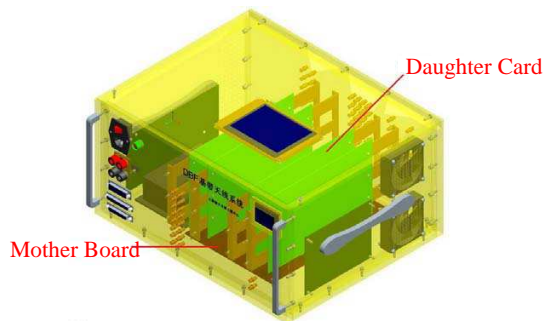
Figure 8. Interconnection structure of BFN hardware platform.

(a)   (b)

Figure 9. Photograph of PCBs: (a) mother board; (b) daughter card.

The hardware platform consists of five PCB boards, including one mother board and four daughter cards. The interconnection structure is presented in Fig. 8. The two wideband signals are driven to the mother board, which performs the functions of A/D converter, DFT filter bank, beaforming computer and calibration in digital domain. Then the processed 61-channel signals are transferred through PCIE interface to four daughter cards, each of which is in charge of 16-channel signals' process. The throughput of data transferred between mother board and four daughter cards should be 34.16 Gbps. PCIE interface is competent for the data transfers with such large number. The photographs of mother board and daughter card are shown in Fig. 9. The daughter card is designed to complete D/A conversion. Because of the limited pins of FPGA, the D/A conversion of 61-channel signals can't be accomplished by one daughter card or the mother board. To make sure that 61-channel signals are transmitted simultaneously, clock and synchronization control signals of four daughter cards are supplied by mother board, as well as the electrical power.

6. CALIBRATION UNIT

Calibration between channels for beamforming system is a critical requirement for accurate performance. It has great influence on beamingforming result. One advantage of DBF systems is the ease in calibration. As the array's transmitting frequency is S band and signal bandwidth is 10 MHz, the system is narrowband. It is possible to apply a single complex weight within each channel to calibrate the entire bandwidth. Phase and amplitude error among channels can be calculated in digital domain via FPGA. The scheme of calibration is shown in Fig. 10.

First, a reference signal is generated on the control of calibration control module. The reference signal is mono-tune signal (cosine
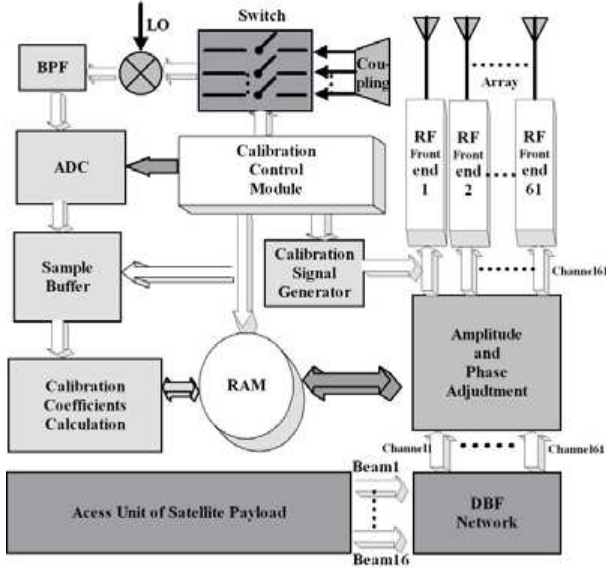
Figure 10. Block diagram of calibration unit.

signal), which centers at 10 MHz and propagates through 61 RF front end channels simultaneously, and it can be expressed as

$$r(n) = \cos(wn) \tag{8}$$

These signals feed back after power amplifier and can be transferred into common down-conversion channel, but only one channel is selected at a time. The access of feedback signal is under the control of calibration control module and exactly carried out by SPDT. After down-conversion, the feedback signal is sampled and fed to the buffer. The feedback signal is expressed as

$$y_i = A \cos(wi - \varphi) + n_i \tag{9}$$

where φ is phase delay of the selected channel, n_i is additive white Gaussian noise of channel response, and A is the amplitude of feedback signal.

Ultimately, the feedback signal is fed to error calculation module, where 61-channel amplitude ratios between the reference signal and the feedback signal of each individual channel are computed based on maximum likelihood criterion. The amplitude response of the selected channel is calculated by function

$$\hat{A} = \frac{2}{N} |Y(w)| = \frac{2}{N} \sum_{i=1}^{N} y_i \tag{10}$$

The phase delay of each channel is also calibrated using similar means. The estimation function of phase response is expressed as

$$\hat{\varphi} = \arctan \left[\frac{\sum_{i=1}^{N} y_i * \sin(wi)}{\sum_{i=1}^{N} y_i * \cos(wi)} \right] \qquad (11)$$

The relative ratios of phase and amplitude response variation among 61 channels can be calculated accordingly, and the magnitude ratios and phase differences are combined into complex-valued error correction weights and latched into RAM. When the phase and amplitude error calculation is completed, calibration unit can access RAM and fetch the calculated phase and amplitude error information to calibrate 61 channels.

The mismatch within 61 RF frontend channels can be removed utilizing the method described above. After calibration, the phase error among channels is limited to 0.5 degree, and the maximum amplitude response difference among channels is 0.2 dB. However, this calibration method only takes RF front end into consideration. The far-field calibration technique will be used to make further phase and amplitude corrections that account for the element pattern and mutual coupling [28, 29].

7. MEASUREMENTS

We have measured the radiation pattern of the DBF transmitter array antenna in an anechoic chamber, the photograph of DBF array antenna under measurement is shown in Fig. 11.

Figure 11. The photograph of DBF array antenna under measurement.
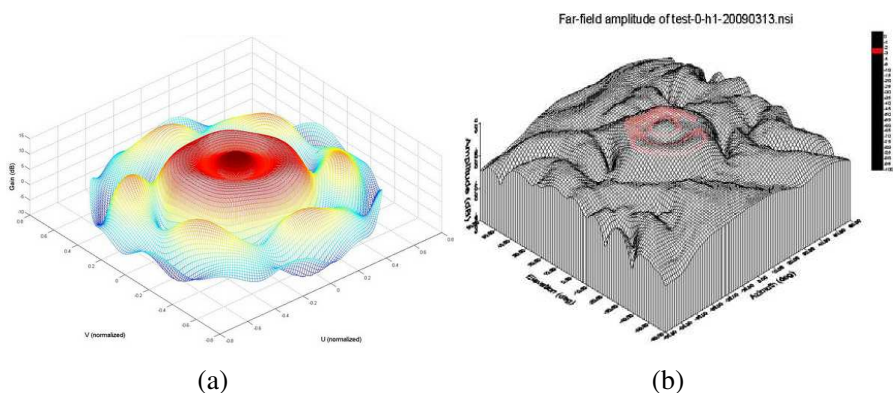
Figure 12. Three-dimensional radiation pattern of main beam: (a) simulation results; (b) measurements.
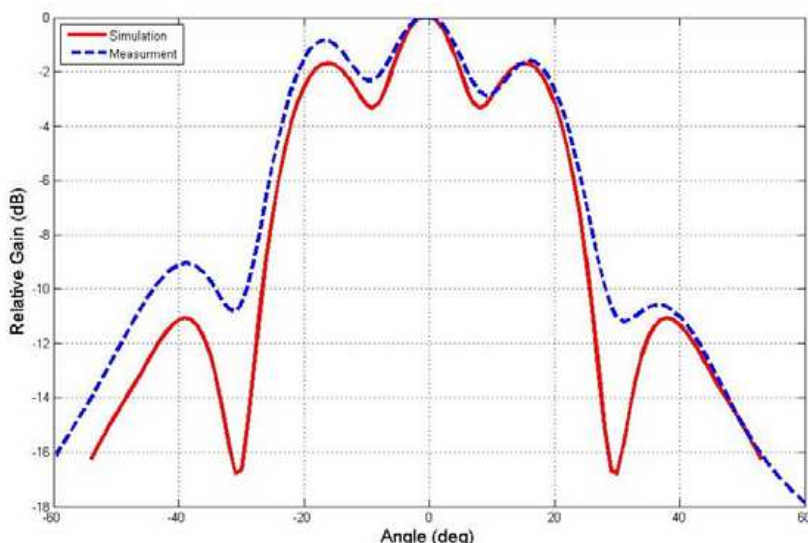
Figure 13. The elevation plane pattern of main beam (normalized).

To measure the parameters of sixteen beams precisely, each beam's radiation pattern was measured individually by supplying the signal input for the measured beam and keeping the other beam's input short circuited to ground. We take two beams as an example: the main beam and one beam in third circle (on the periphery of beam coverage), and the measured result and simulation result are shown in Fig. 12.
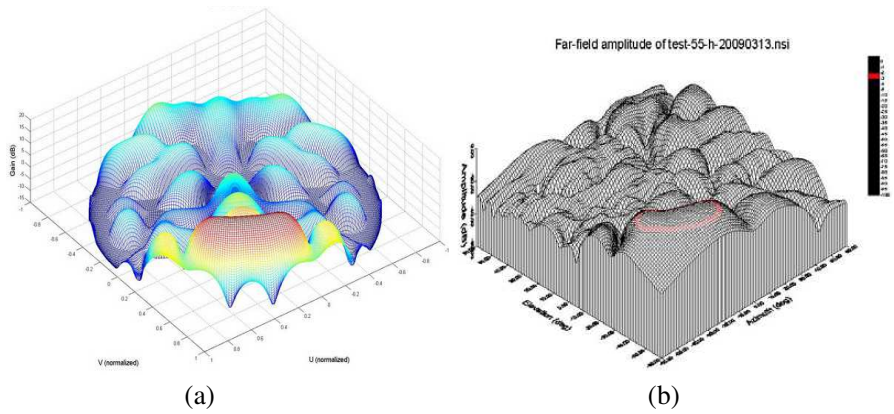
Figure 14. Three-dimensional radiation pattern of one beam in the third circle: (a) simulation results; (b) measurements.
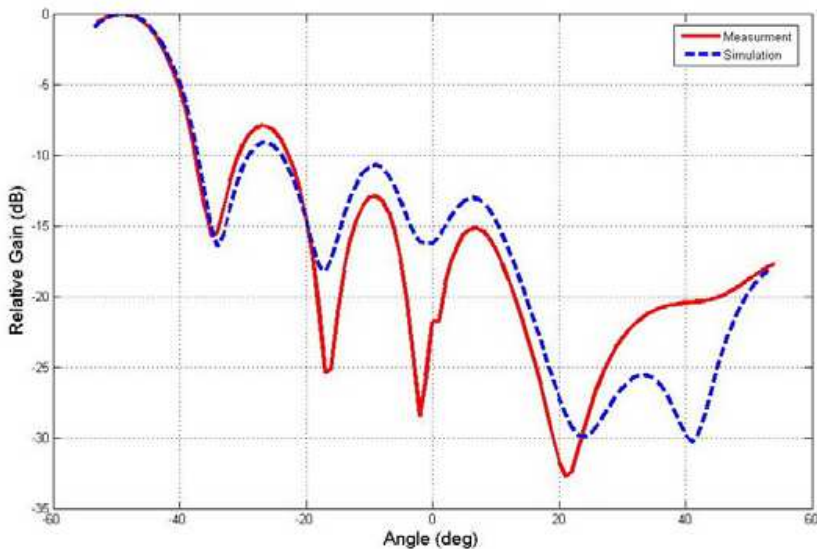
Figure 15. The elevation plane pattern of one beam in the third circle.

From Fig. 12 to Fig. 15, it can be concluded that the DBF array antenna has pretty good performance of beamforming capability, and the measured result agrees well with the simulation result. The three-dimensional radiation pattern of measurements is similar with that of simulation, especially in the aspect of mainlobe's shape and

distribution. The directivity variation in maximum gain point of main beam is $(\Delta\theta, \Delta\varphi) = (0, 0)$, whereas the variation of the beam in the third beam is $(\Delta\theta, \Delta\varphi) = (0.4°, 0.6°)$. Moreover, the beamforming result of mainlobe is better than that of sidelobe, with the measured sidelobes levels of presented beam a bit higher than the simulation result. The pattern gain error may be caused by two reasons. One is the quantification error of DBF network; the other is the non-consistency of RF front-end channels and mutual coupling effect of antenna elements. Further research work will be done to reduce the influences of these factors.

8. CONCLUSION

A 61-channel DBF transmitter array antenna for mobile satellite communication is presented in this paper. It is a useful approach to control the radiation pattern by dint of digital processing at IF, as verified by the measurements. Ultimately, the measurements of array antenna show good agreement with the simulation result, which validates the rationality and feasibility of algorithms and project design. The successful implementation of DBF array enhances the possibility of DBF array antenna utilized for a new generation of Chinese LEO satellite.

REFERENCES

1. Athanasopoulos, N. C. and N. K. Uzunoglu, "Development of a 10 GHz phased array cylindrical antenna system incorporating IF phase processing," *Progress In Electromagnetics Research*, PIER 59, 17–38, 2006.
2. Chiba, I., R. Miura, and T. Tanaka, "Digital beam forming (DBF) antenna system for mobile communications," *IEEE Transactions on Aerospace and Electronic Systems*, Vol. 12, No. 9, 31–41, 1997.
3. Roy, S. D. and S. Kundu, "Performance analysis of cellular CDMA in presence of beam forming and soft soft hand off," *Progress In Electromagnetics Research*, PIER 88, 73–89, 2008.
4. Martin, M. J., C. Montesano, G. A. E. Crone, and R. Garcia, "ASYRIO: Antenna system reconfiguration in orbit," *IEEE Transaction on Antennas and Propagation*, Vol. 37, No. 3, 7–14, 1995.
5. Dreher, A., N. Niklasch, and F. Klefenz, "Antenna and receiver system with digital beam forming for satellite navigation and

communications," *IEEE Transactions on Microwave Theory and Techniques*, Vol. 51, No. 7, 1815–1821, 2003.

6. Kuwahara, Y., H. Kakinuma, and S. Ogawa, "Development and evaluation test of DBF equipment for transmitting," *IEEE AP-S1999*, Florida, USA, 1999.

7. Curtis, D. D. and R. W. Capt, "32-channel X-band digital beamforming plug-and-play receive array," *IEEE Symposium on Phased Array Systems and Technology*, Boston, USA, 2003.

8. Harry, L. and V. Trees, *Optimum Array Processing Part IV of Detection, Estimation, Modulation Theory*, John Wiley & Sons, New York, 2008.

9. Yang, S., Q. Z. Liu, J. Yuan, and S.-G. Zhou, "Fast and optimal design of a K-band transmit-receive active antenna array," *Progress In Electromagnetics Research B*, Vol. 9, 281–299, 2008.

10. Eldek, A. A. and A. Z. Elsherbeni, "Rectangular slot antenna with patch stub for ultra wideband applications and phased array systems," *Progress In Electromagnetics Research*, PIER 53, 227–237, 2005.

11. OuYang, J., "A novel radiation pattern and frequency reconfigurable microstrip antenna on a thin substrate for wide-band and wide-angle scanning application," *Progress In Electromagnetics Research Letters*, Vol. 4, 167–172, 2008.

12. Qu, Y., G. Liao, and S. Q. Zhu, "Pattern synthesis of planar antenna array via convex optimization for airborne forward looking radar," *Progress In Electromagnetics Research*, PIER 84, 1–10, 2008.

13. Brégains, J. C. and J. A. Rodríguez, "Optimal synthesis of line source antennas based on rhodes distributions," *Progress In Electromagnetics Research*, PIER 36, 1–19, 2002.

14. Sukharevsky, O. I. and A. Y. Shramkov, "High-frequency method of antenna directional pattern calculation," *Journal of Electomagnetic Waves and Application*, Vol. 21, No. 14, 2009–2023, 2007.

15. Mahanti, G. K. and A. Chakrabarty, "Phase-only and amplitude-phase only synthesis of dual-beam pattern linear antenna arrays using floating-point genetic algorithms," *Progress In Electromagnetics Research*, PIER 68, 247–259, 2007.

16. Jeong, Y. S. and J. H. Lee, "Estimation of time delay using conventional beamforming-based algorithm for UWB systems," *Journal of Electomagnetic Waves and Application*, Vol. 21, No. 15, 2413–2420, 2007.

17. Xu, Z., H. Li, Q. Z. Liu, and J. Y. Li, "Pattern synthesis of conformal antenna array by the hybrid genetic algorithm," *Progress In Electromagnetics Research*, PIER 79, 75–90, 2008.

18. Li, W. T., X. W. Shi, and L. Xu, "Improved GA and PSO culled hybrid algorithm for antenna array pattern synthesis," *Progress In Electromagnetics Research*, PIER 80, 461–476, 2008.

19. Capozzoli, A. and G. D'Elia, "Global optimization: Applications to advanced reflector antennas synthesis and diagnosis techniques," *Progress In Electromagnetics Research*, PIER 56, 195–232, 2006.

20. Rostami, A. and A. Yazdanpanah-Goharrizi, "Hybridization of neural networks and genetic algorithms for identification of complex Bragg gratings," *Journal of Electomagnetic Waves and Application*, Vol. 22, No. 5–6, 643–664, 2008.

21. Reyna, A. and M. A. Panduro, "Optimation of a scannable pattern for uniform planar antenna arrays to minimize the side lobe level," *Journal of Electomagnetic Waves and Application*, Vol. 22, No. 16, 2241–2250, 2008.

22. Crochiere, R. E., *Mutirate Digital Signal Processing*, Prentice-Hall Press, New Jersey, 2001.

23. Lim, Y. C. and Y. J. Yu, "Optimum masking levels and coefficient sparseness for Hilbert transformers and half-band filters designed using the frequency-response masking technique," *IEEE Transaction on Circuits and Systems*, Vol. 52, No. 11, 2444–2453, 2005.

24. Zhang, X., Z. Wang, and D. Xu, "Wavelet packet transform-based least mean square beamformer with low complexity," *Progress In Electromagnetics Research*, PIER 86, 291–304, 2008.

25. Meng, C. C. and T. H. Wu, "2.4/5.7 GHz CMOS dual-band low-IF architecture using weaver-hartley image-rejection techniques," *IEEE Transaction on Microwave Theory and Techniques*, Vol. 57, No. 3, 552–561, 2009.

26. Panduro, M. A. and C. Bocio, "Design of beam-forming networks for scannable multi-beam antenna arrays using corps," *Progress In Electromagnetics Research*, PIER 84, 173–188, 2008.

27. Mahanti, G. K., A. Chakraborty, and S. Das, "Design of fully digital controlled reconfigurable array antennas with fixed dynamic range ratio," *Journal of Electomagnetic Waves and Application*, Vol. 21, No. 1, 97–106, 2007.

28. Alfred, Q. M., T. Chakravarty, and S. K. Sanyal, "A novel schematic for calibration of large phased array antenna using

programmable time-delay units," *Progress In Electromagnetics Research*, PIER 65, 81–91, 2006.

29. Yuan J., Y. Qiu, and Q. Z. Liu, "Fast analysis of multiple antennas coupling on very electrical large objects via parallel technique," *Journal of Electomagnetic Waves and Application*, Vol. 22, No. 8–9, 1232–1241, 2008.